

Original article

Differential diagnosis of lung cancer and tuberculosis based on ¹⁸F-fluorodeoxyglucose PET/CT multi-time points imaging

Yongjun Luo^{a,b,c,d,*}, Jicheng Li^{b,c,d}, Wanjun Ma^{b,c,d,*}, Xiaoxue Tian^{b,c,d,*},
Lele Huang^{b,c,d}, Han Yuping^{b,c,d}, Kai Zhang^{b,c,d}, Yijing Xie^{a,c,d}, Zhencun Cui^{b,c,d},
Jianzhong Feng^{b,c,d} and Junlin Zhou^{a,c,d}

Objective To investigate the value of ¹⁸F-fluorodeoxyglucose (FDG) PET/CT multi-time points imaging (MTPI) on the differential diagnosis between lung cancer (LC) and tuberculosis (TB).

Methods Sixty-four patients underwent ¹⁸F-FDG PET/CT MTPI. The stdSUVmax, stdSUVavg, retention index, metabolic tumor volume, total lesion glycolysis at four-time points and slope of metabolic curve were measured and calculated, and the sex, age, and uniformity of FDG uptake were recorded. The difference in each index between LC and TB was analyzed, and dynamic metabolic curves (DMCs) of LC and TB were fitted by significance indexes. Artificial neural network (ANN) prediction models were established between squamous cell carcinoma (SCC) and TB, as well as between adenocarcinomas and TB.

Results Differences between SCC and TB, stdSUVmax/avg at four-time points, total lesion glycolysis, stdSUVmax/avg slope (1–2 h, 1–3 h and 1–4 h), uniformity of FDG uptake and age were significant. stdSUVavg has the largest area under the 4 h curve; age was only significant between adenocarcinomas and TB. DMCs at 1–4 h fitted by stdSUVavg were more helpful in differentiating LC and TB than stdSUVmax. stdSUVavg (1 h and 4 h), stdSUVavg slope 1–4 h, age, and uniformity of FDG uptake were selected to establish an ANN prediction

model between SCC and TB; the area under the curve (AUC) was 100.0%. The same indices were used to establish the prediction model between adenocarcinomas and TB; the AUC was up to 83.5, and after adding stdSUVavg (2 and 4 h) to adenocarcinomas and TB models, the AUC was 87.7%.

Conclusion ¹⁸F-FDG PET/CT MTPI fitting DMCs and establishing an ANN prediction model would distinguish SCC from TB relatively accurately and provide certain help in the differentiation between adenocarcinomas and TB. *Nucl Med Commun* 44: 732–740 Copyright © 2023 Wolters Kluwer Health, Inc. All rights reserved.

Nuclear Medicine Communications 2023, 44:732–740

Keywords: ¹⁸F-FDG PET/CT, adenocarcinoma, artificial neural network, dynamic metabolic curve, squamous cell carcinoma, tuberculosis

Departments of ^aRadiology, ^bNuclear Medicine, Lanzhou University Second Hospital, ^cSecond Clinical School, Lanzhou University and ^dKey Laboratory of Medical Imaging of Gansu Province, Lanzhou, China

Correspondence to Junlin Zhou, MD, PhD, Department of Radiology, Lanzhou University Second Hospital, Cuiyingmen No.82, Chengguan District, Lanzhou 730030, China
Tel: +86 135 1961 2787; fax: +86 931 894 2595;
e-mail: ery_zhoujl@lzu.edu.cn

*Yongjun Luo, Jicheng Li, Wanjun Ma and Xiaoxue Tian contributed equally to the writing of this article.

Received 24 November 2022 Accepted 9 May 2023.

Introduction

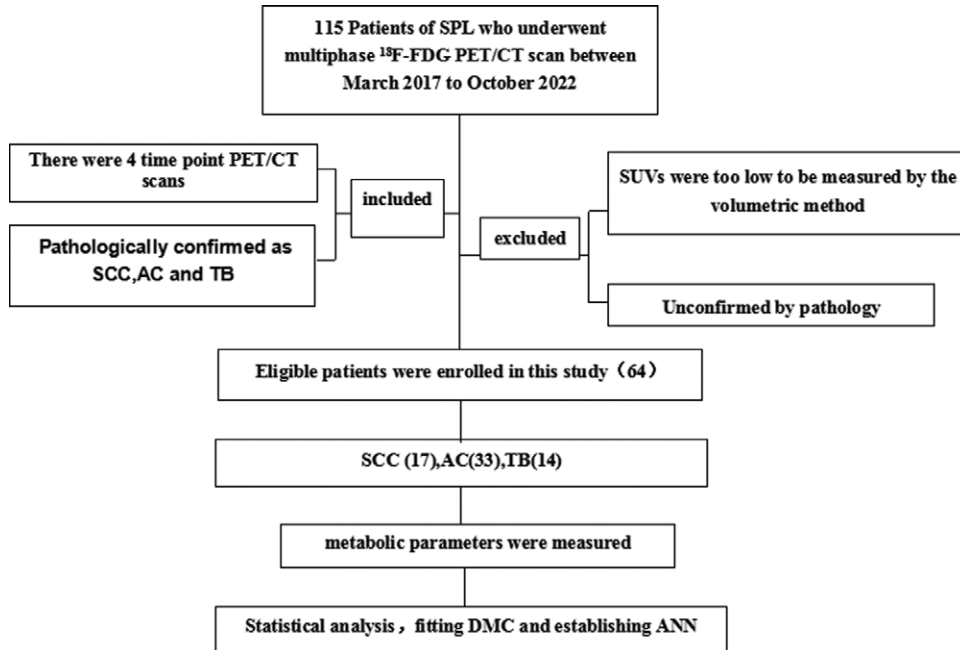
While coronavirus disease (COVID-19) has been sweeping the world in recent years, tuberculosis (TB) and lung cancer (LC) are still the major diseases threatening human health and death, which are often challenging to distinguish owing to their similar imaging manifestations [1]. Accurate diagnosis is important for reducing patient pressure and guiding clinical treatment. As an important research tool, PET/CT has high detection sensitivity, but routine examination lacks specificity [2].

A previous study [3] performed ¹⁸F-fluorodeoxyglucose (FDG) PET/CT multi-time points imaging (MTPI) of solitary pulmonary lesions (SPLs) to identify their benign and malignant status, and only metabolic parameters and clinical features not susceptible to human factors were selected for analysis. This study found that stdSUVavg at

different time points were more valuable in the differentiation of benign and malignant SPLs. A set of parameters related to stdSUVavg were selected to fit the dynamic metabolic curves (DMCs) and establish the artificial neural network (ANN) models, which showed good diagnostic efficiency. This previous study also preliminarily drew the DMCs of SPLs of different pathological types, which showed a significant difference between squamous cell carcinoma (SCC) and TB, while adenocarcinomas (AC) and TB were similar to each other and slightly different.

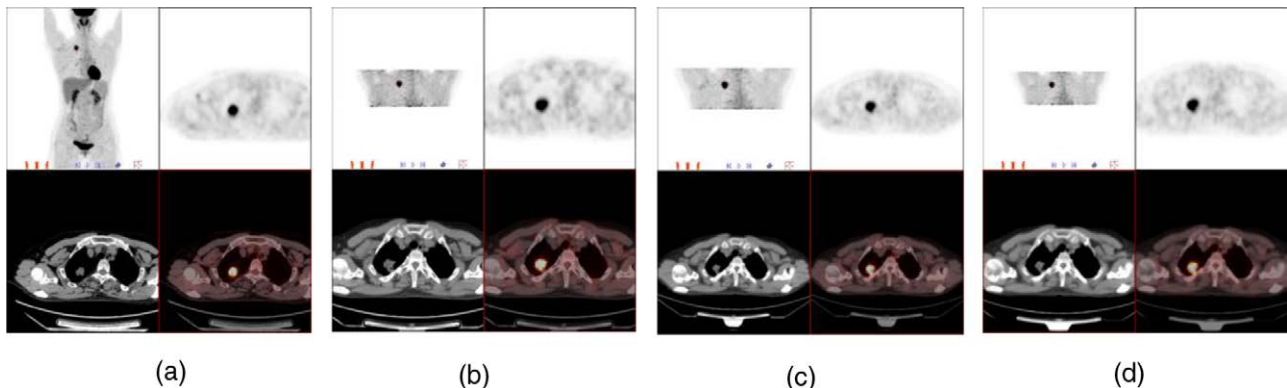
Based on previous studies, this study sorted out the latest data, screened SCC, AC, and TB meeting the inclusion criteria, and analyzed the differences between SCC and TB, AC and TB using similar research methods [3] to provide a more accurate and specific reference basis for the differential diagnosis of SPLs.

Fig. 1



Flow diagram of the recruitment pathway.

Fig. 2



PET/CT examination. Whole body scanning (a). Local delayed scanning of SPL at 2 h (b), 3 h (c), and 4 h (d).

Methods

Patient and inclusion criteria

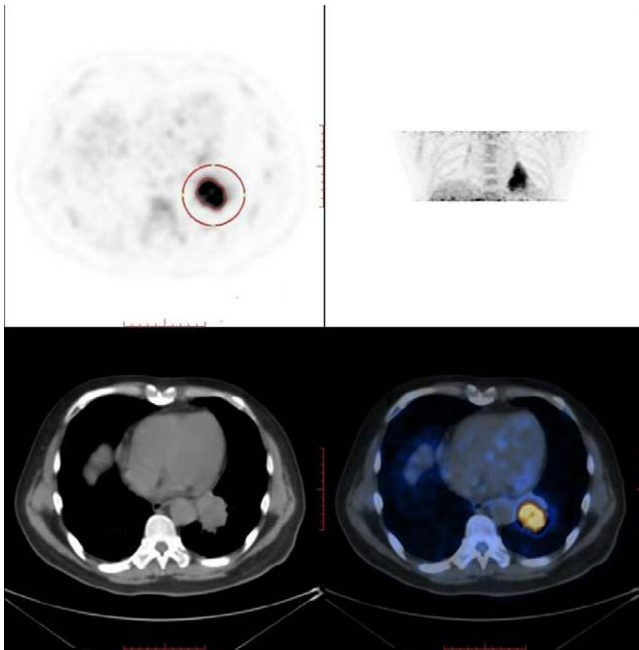
This study was reviewed and approved by the Ethics Committee of the Second Hospital of Lanzhou University, and the previous study and the latest data were reorganized to conduct a retrospective study. A total of 115 SPLs patients who received ^{18}F -FDG PET/CT MTPI from March 2017 to November 2022 were collected, and each patient signed an informed consent form. The inclusion criteria were: (1) complete scan at four-time points and (2) confirmed by pathology. The exclusion criteria were

as follows: (1) The SUV was too low to be measured by the 3D marking method, and (2) it was not confirmed by pathology. Finally, 64 patients (17 SCC, 33 AC, and 14 TB) were analyzed (Fig. 1).

PET/CT examination

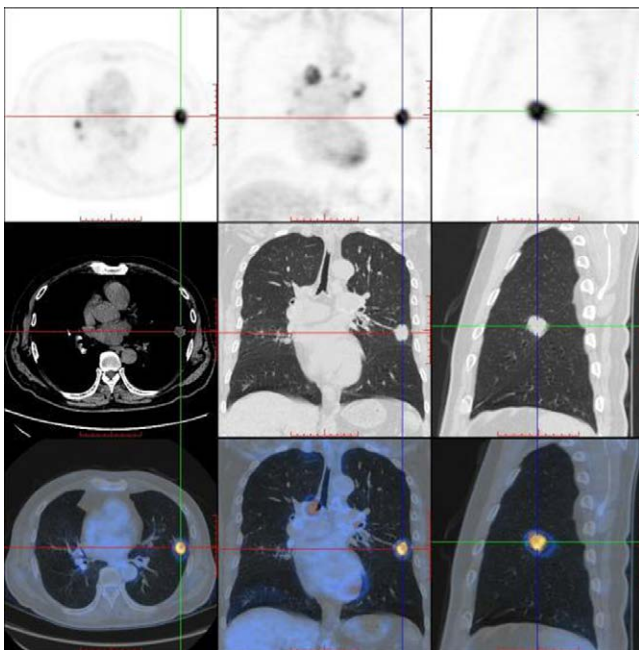
The scanning method was similar to that used in a previous study [3] and referenced the European Association of Nuclear Medicine procedure guidelines for tumor imaging [4]. Patients fasted for 4–6 h (h) before the examination, and the blood glucose concentration was controlled

Fig. 3



PET/CT Image measurements. 3D-labeled lesion method.

Fig. 4

Uniformity of FDG uptake of a 53-year-old male patient with SCC. Localized low uptake of ^{18}F -FDG. SCC, squamous cell carcinoma.

within 8.0 mmol/l, and the maximum was no more than 11.1 mmol/L. Patients were advised to wear loose clothes, not wear metal objects, rest quietly, and avoid light for

10 min. Patients were then administered ^{18}F -FDG intravenously; the injection dose was 0.10 mCi/kg. After injection, patients were to lie in repose for 1 h, urinate, and then perform a routine PET/CT scan from the top of the skull to the mid-upper thigh. Under the conditions of spiral CT scanning, the voltage was 120 KVP, 80–240 mA was automatically switched, the layer thickness was 3.75 mm, the rotation speed was 0.6 s/week, the pitch was 1.0/s, and the matrix was 512×512 . A matrix of 128×128 was used for PET emission scanning, 1 min was collected for each bed, and 6–8 beds were scanned for the whole body (Fig. 2a). Local delayed scanning of SPL was performed at 2 h (Fig. 2b), 3 h (Fig. 2c), and 4 h (Fig. 2d) after ^{18}F -FDG injection to obtain PET-CT images.

PET/CT image measurements and definition of uptake uniformity

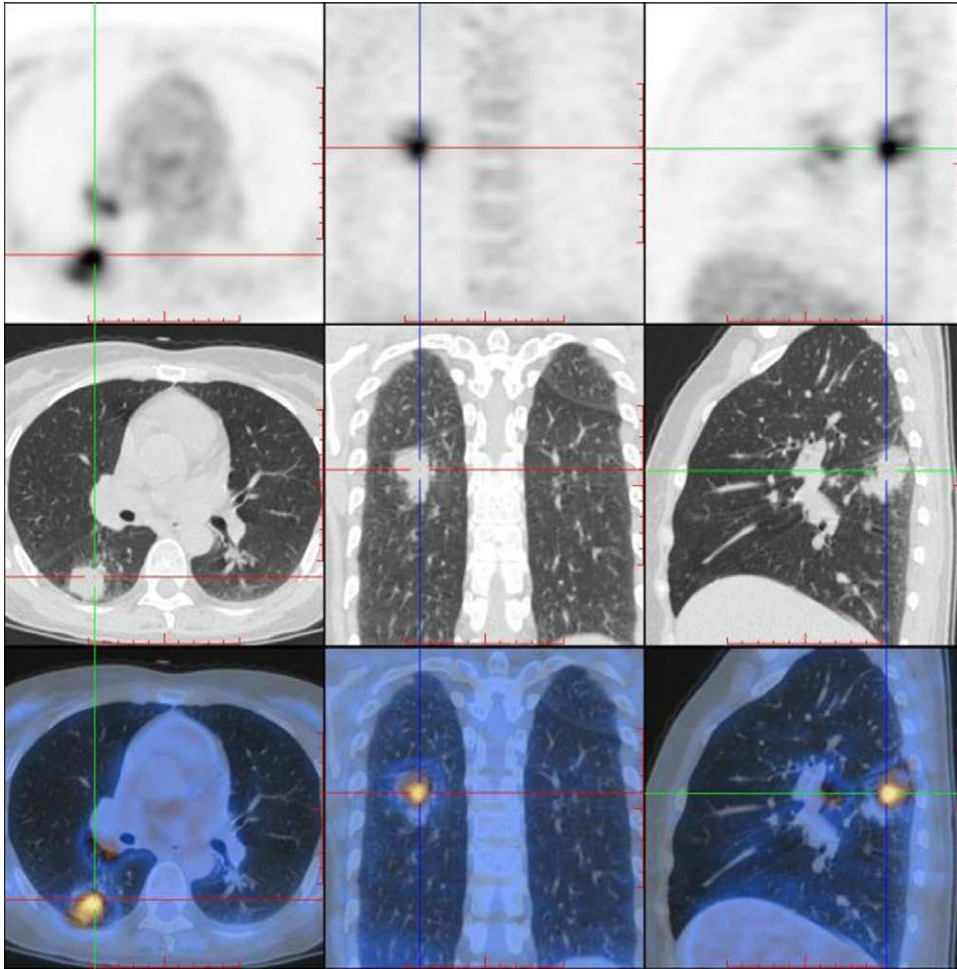
All measurements method were similar to those taken in previous studies [2]. The 3D-labeled lesion method was performed on GE Healthcare's AW4.6 workstation by two nuclear medicine physicians with more than 3 years of experience in PET/CT diagnosis (Fig. 3). The SUVmax was measured at the aortic arch for 1 h (taking the average of the three measurements). Standardized SUV values (stdSUVmax, lesion SUVmax/mediastinal 1 h SUVmax; stdSUVavg, lesion SUVavg/mediastinal 1 h SUVmax), retention index [RI; (delayed SUVmax-early SUVmax)/early SUVmax $\times 100\%$], metabolic tumor volume (MTV; measured using the extracted lesion volume greater than 40% of the maximum SUV value), total lesion glycolysis (TLG) and slope of metabolic curve (1-2h, 1-3h, 1-4h, 2-3h, 2-4h, 3-4h) were measured and calculated. Localized low uptake of ^{18}F -FDG in visual observation lesions is uneven (Fig. 4), and homogeneous uptake is even (Fig. 5).

Statistical analysis

The data were analyzed by SPSS 26.0 statistical analysis software. Each metabolic parameter of SCC, AC, and TB groups was compared. Quantitative data of normal distribution was analyzed using one way of variance, while the Kruskal-Wallis H test analyzed the skew distribution of the data. The receiver operating characteristic (ROC) curve was drawn for statistically significant variables to evaluate the diagnostic effect of various indicators between LC and pulmonary TB. The area, sensitivity, specificity, Youden index, and other indicators under the ROC curve were used to evaluate the diagnostic effect (Fig. 6), and the significance level was 0.05.

We selected stdSUV values with statistical significance and high diagnostic efficiency between SCC or AC and TB to fit the DMCs. The parameters with statistical significance and high diagnostic efficiency were screened, and the ANN prediction models of LC and TB (SCC and TB, AC and TB) were established using the radial basis

Fig. 5



Uniformity of FDG uptake of a 47-year-old female patient with TB. Homogeneous uptake of ^{18}F -FDG. TB, tuberculosis.

function of the ANN. The index screened during the establishment of the model was taken as the input neuron and SCC, AC, or TB was taken as the output neuron. The codes were 1, 2, and 3, respectively. The ratio of the training set to the test set was 7:3. Case processing summary, independent variables importance analysis, model summary, ROC curve, classification results, and predicted observed chart were selected and output; others were system default. The diagnostic efficiency of the model was evaluated by the ROC curve, sensitivity, specificity, positive predictive value, negative predictive value, accuracy, and other indicators.

Results

Clinical and metabolic characteristics

The stdSUVmax (at 1 h, 2 h, 3 h, and 4 h), stdSUVavg (at 1 h, 2 h, 3 h, and 4 h), TLG (at 1 h, 2 h, 3 h, and 4 h), stdSUVmax slope (between 1–2 h, 1–3 h, and 1–4 h), stdSUVavg slope (between 1–2 h, 1–3 h, and 1–4 h), uniformity of FDG uptake, and age between SCC and TB were

statistically different; there was only a statistical difference in age between AC and TB, and no statistical difference in other metabolic parameters.

Diagnostic performance

Among all the indicators with statistical differences, the area under the curve (AUC) of stdSUVmax (at 1 h, 2 h, 3 h, and 4 h) and stdSUVavg (at 1 h, 2 h, 3 h, and 4 h) were higher, reaching more than 90%, and the AUC of stdSUVavg between 1–4 h was higher than that of others, and the AUC of stdSUVavg at 4 h was the largest. When the stdSUVmax (at 1 h, 2 h, 3 h, and 4 h) thresholds were 6.74, 7.87, 6.78, and 9.22, the diagnostic sensitivity was 76.5%, 76.5%, 94.1%, and 71.4%, respectively; the specificity was 92.9%, 92.9%, 71.4%, and 92.9%, respectively; and when the stdSUVavg (at 1 h, 2 h, 3 h, and 4 h) threshold was 3.35, 4.41, 4.58, 4.57, 3, the diagnostic sensitivities were 82.4, 76.5, 76.5, and 82.4%, respectively. The specificities were 92.9, 100.0, 100.0, and 100.0% (Table 1). It could be seen that the sensitivity

and specificity of stdSUVavg at 1 h and stdSUVavg at 4 h were relatively high.

Dynamic metabolic curves

The DMCs (SCC, AC, and TB) fitted by stdSUVmax (at 1 h, 2 h, 3 h, and 4 h) showed SCC and TB were significantly different, however, the AC and TB were similar and particularly close, which was not easy to distinguish. (Fig. 7a); the same data were used to fit the DMCs between AC and TB, the curve of TB was slightly higher than that of AC, with little difference (Fig. 7b). When taking the stdSUVavg (at 1 h, 2 h, 3 h, and 4 h) to fit the DMCs of SCC, AC, and TB, the difference between SCC and TB was more obvious; the curve also differed between AC and TB, the curve of

AC was slightly higher than that of TB (Fig. 7c), and the difference between the curves of AC and TB was more obvious when fitted separately with the same data (Fig. 7d).

Artificial neural network

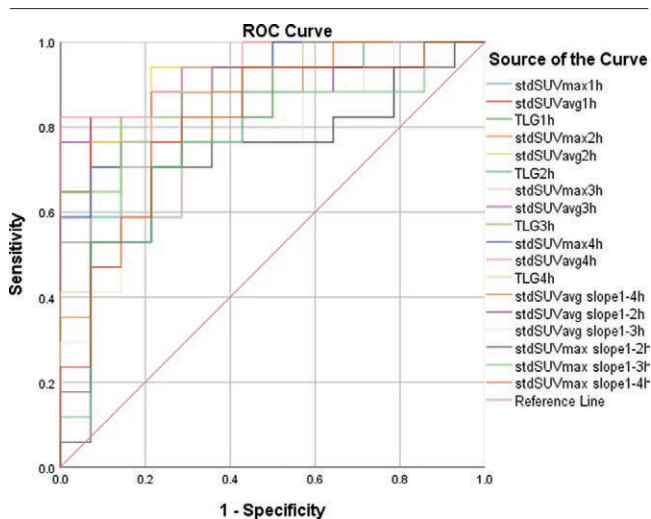
The SCC and TB ANN prediction model was established with indicators stdSUVavg (at 1 h and 4 h), stdSUVavg slope between 1–4 h, age, and uniformity of FDG uptake of statistical difference between SCC and TB, Neural networks model architectures (radial basis function) such as Fig. 8, the AUC was 100.0% (Fig. 9a). The prediction model between AC and TB (model 1) was established with the same index of SCC and TB, the highest AUC was 83.5 (Fig. 9b); after adding stdSUVavg at 2 h and stdSUVavg at 3 h into the AC and TB model (model 2), the AUC reached 87.7% (Fig. 9c).

After automatically learning its rules from the training set, the test set was tested to evaluate the prediction accuracy of the ANN model. The positive and negative predictive values and overall accuracy of SCC and TB models were 100.0%. The positive predictive value of the AC and TB model was 100.0%, the negative predictive value was 33.3%, and the overall accuracy was 85.7% (Table 2). Analysis of SCC and TB, AC, and TB model abstracts revealed that the percentage of incorrect predictions of the training and testing samples were similar (Table 3).

Discussion

This study passed the ethical approval of the Second Hospital of Lanzhou University. We screened patients with solitary pulmonary nodules or masses, who had no other apparent lesions in the whole body, and were in a generally good condition and had come to our department for differential diagnosis by PET/CT examination. After signing the informed consent letter for MTPI, the PET/

Fig. 6



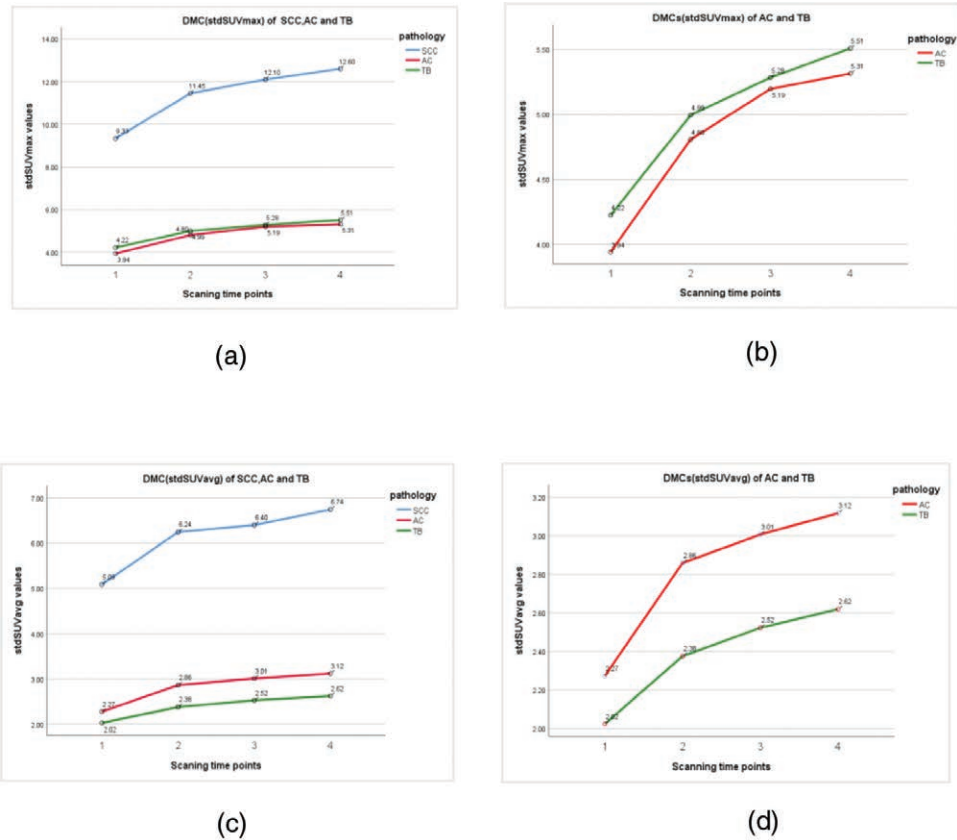
ROC of each metabolic parameter.

Table 1 Diagnosis efficacy of each metabolic parameters between LC and TB

Variable	Optimal cutoff values	AUC (95% CI)	P	Youden index	Sensitivity (%)	Specificity (%)
stdSUVmax 1h	6.74	0.908 (0.809–1.000)	0.000	0.694	0.765	0.929
stdSUVmax 2h	7.87	0.903 (0.800–1.000)	0.000	0.694	0.765	0.929
stdSUVmax 3h	6.78	0.903 (0.800–1.000)	0.000	0.655	0.941	0.714
stdSUVmax 4h	9.22	0.899 (0.795–1.000)	0.000	0.635	0.706	0.929
stdSUVavg 1h	3.35	0.912 (0.806–1.000)	0.000	0.753	0.824	0.929
stdSUVavg 2h	4.41	0.924 (0.800–1.000)	0.000	0.765	0.765	1.000
stdSUVavg 3h	4.58	0.908 (0.796–1.000)	0.000	0.765	0.765	1.000
stdSUVavg 4h	4.57	0.929 (0.837–1.000)	0.000	0.824	0.824	1.000
TLG1h	141.07	0.845 (0.708–0.981)	0.001	0.635	0.706	0.929
TLG2h	100.23	0.866 (0.740–0.991)	0.001	0.622	0.765	0.857
TLG3h	99.41	0.891 (0.775–1.000)	0.000	0.681	0.724	0.857
TLG4h	99.68	0.866 (0.739–0.992)	0.001	0.622	0.765	0.857
stdSUVmax slope 1–2h	1.20	0.723 (0.535–0.910)	0.009	0.492	0.706	0.786
stdSUVmax slope 1–3h	0.90	0.765 (0.590–0.939)	0.015	0.492	0.706	0.786
stdSUVmax slope 1–4h	0.61	0.811 (0.655–0.967)	0.002	0.551	0.765	0.786
stdSUVavg slope 1–2h	0.48	0.777 (0.611–0.943)	0.035	0.479	0.765	0.714
stdSUVavg slope 1–3h	0.54	0.765 (0.587–0.926)	0.012	0.445	0.588	0.857
stdSUVavg slope 1–4h	0.20	0.824 (0.679–0.968)	0.003	0.525	0.882	0.643

AC, adenocarcinoma; LC, lung cancer; MTV, metabolic tumor volume; RI, retention index; SCC, squamous cell carcinoma; stdSUVavg, SUVavg/aortic arch SUVmax(1h); stdSUVmax, SUVmax/aortic arch SUVmax(1h); TB, tuberculosis; TLG, total lesion glycolysis.

Fig.7



DMCs of SCC, AC, and TB. DMC (stdSUVmax) of SCC, AC, and TB (a); DMC (stdSUVmax) of AC and TB (b); DMC (stdSUVavg) of SCC, AC, and TB (c); DMC (stdSUVavg) of AC and TB (d). SCC, squamous cell carcinoma; TB, tuberculosis.

CT examination was arranged at a relatively fixed time in the morning, which did not affect the regular work of the department. The first scan covered the routine head-to-thigh root, and the three delayed imaging covered the local low-dose scanning of pulmonary lesions, with a total of about ten beds. After every scanning, patients were sent to a waiting room to lie down and rest. All the examinations could be completed during off-duty or at noon.

Various imaging examinations and studies have advantages and disadvantages in the differential diagnosis of SPLs, such as LC and TB [2,5–12]. Previous studies analyzed the benign and malignant identification of SPL [3]. This study further analyzed the characteristics of ^{18}F -FDG PET/CT MTPI of LC and TB, striving to find more accurate, effective, and clinically practical diagnostic methods and apply them to clinical practice.

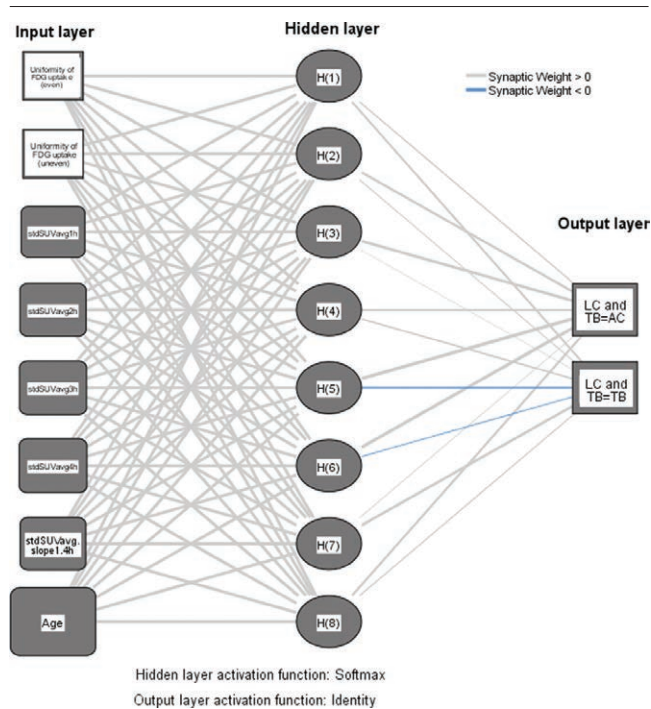
To reduce the differences between different observer, and the influencing factors of SUV, we used the 3D-labeled lesion method to measure and calculate the stdSUV, RI, MTV, and TLG; age and sex were recorded. Previous studies showed that malignant SPLs were more prone to uneven uptake than benign SPLs [3]. A recent study on this manifestation showed

that uneven low uptake in solid TB is generally biased, and uneven low uptake in non-small cell LC is generally centered [6], suggesting that there are certain differences in uniformity of FDG uptake between benign and malignant SPLs. This study continues to include uniformity of FDG uptake as an indicator, and the difference in each indicator between SCC and TB, AC and TB were analyzed. Valuable indicators for statistical and clinical comprehensive analysis were selected to fit the DMCs and establish the ANN models, to find a more effective and accurate method for the differential diagnosis of LC and TB.

Solid nodules of TB are also a type of granuloma, and the uptake of ^{18}F -FDG is similar to that of LC [13]. Most previous studies have generally classified SPL of different pathological types as benign or malignant for differential diagnosis. Even if TB is differentiated from LC, non-small cell LC is classified into one category [3,5,6,14], thus, the metabolic values of different pathological types of SPL are integrated, weakening the characteristics of different SPL to a certain extent.

In this study, we found that stdSUVmax (at 1 h, 2 h, 3 h, and 4 h), stdSUVavg (at 1 h, 2 h, 3 h, and 4 h), TLG (at

Fig. 8



Neural networks (radial basis function).

1 h, 2 h, 3 h, and 4 h), stdSUVmax slope (between 1–2 h, 1–3 h, and 1–4 h), stdSUVavg slope (between 1–2 h, 1–3 h, and 1–4 h), uniformity of FDG uptake, and age showed a statistical difference between SCC and TB, while only age showed a statistical difference between AC and TB. It was speculated that the difference between LC and TB was not easy to distinguish between AC and TB; the larger the proportion of AC in benign and malignant SPL included in relevant research data, the more difficult it may be to differentiate.

The results of this study showed that the AUC of stdSUVmax (at 1 h, 2 h, 3 h, and 4 h) and stdSUVavg (at 1 h, 2 h, 3 h, and 4 h) between SCC and TB was more than 90%, and the diagnostic efficiency of stdSUVavg at 4 h was the highest, indicating that stdSUVavg has a higher value in the differential diagnosis of SPL. This is similar to the results of our previous research [3]. It was suggested that the stdSUV has higher diagnostic efficiency than the SUV, which can be easily applied in clinical practice by manual calculation.

Studies [15] have shown that MTV was more valuable among malignant pulmonary nodules that were smaller than 2 cm, and no difference in SUVmax, MTV, and TLG was observed with an increase in SPN diameter and density. In this study, MTV showed no statistical difference between LC and TB but showed a gradually increasing trend from 1 to 4 h. Furthermore, TLG demonstrated a similar trend, increased gradually from

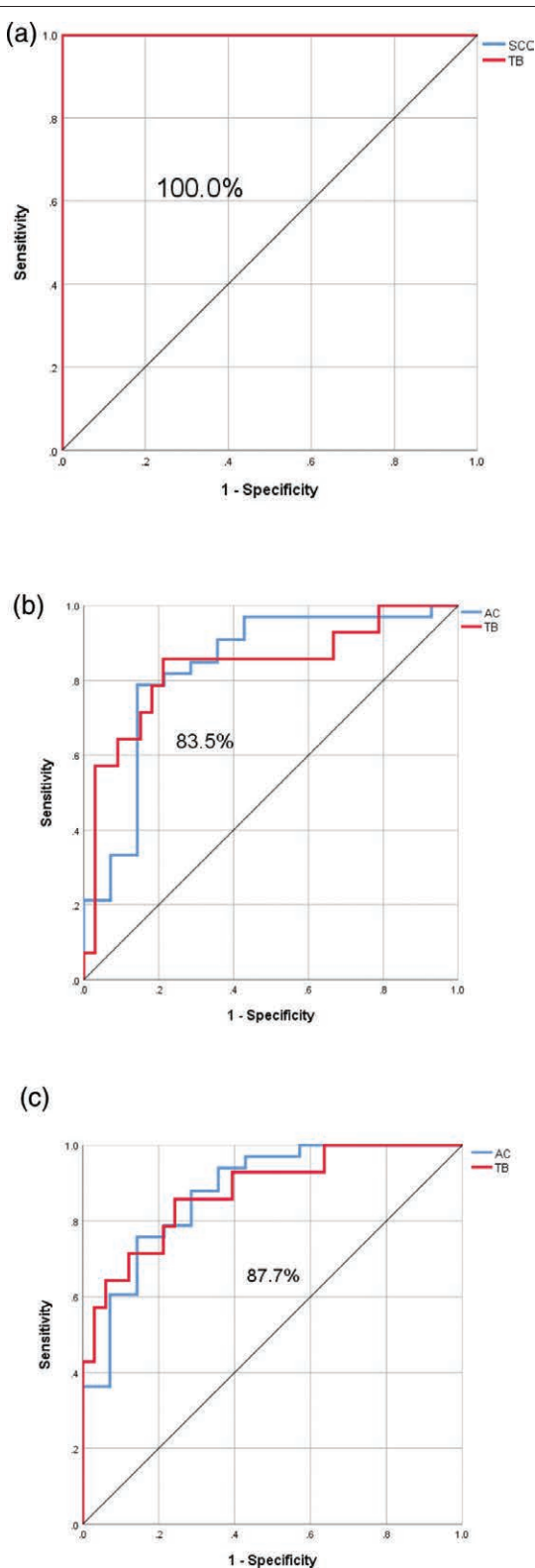
1 to 3 h, and remained stable after 4 h. However, a statistical difference between SCC and TB was observed for TLG. Further, TLG is derived from the product of MTV and SUVavg. An increase in TLG indirectly reflects an increase in MTV, indicating that TLG is also valuable in the identification of benign and malignant tumors. Moreover, MTV and TLG are valuable for differentiating between benign and malignant tumors, and they have also been applied in studies related to the differentiation of benign and malignant bone tumors [16]. A previous study [3] showed that SUVmax demonstrated statistical differences in identifying benign and malignant SPLs; however, stdSUV had a higher value and more stable efficacy, especially stdSUVavg, so only stdSUV was included in this study for analysis. This study showed that stdSUVavg at 4 h had the highest AUC value. Therefore, stdSUVavg at four-time points was selected to fit the DMC. A group of metabolic parameters related to stdSUVavg was selected to establish an ANN model, and its diagnostic effect was observed.

We used stdSUVmax (at 1 h, 2 h, 3 h, and 4 h) and stdSUVavg (at 1 h, 2 h, 3 h, and 4 h) to fit the DMCs for observation and found that the DMCs of stdSUVmax (at 1 h, 2 h, 3 h, and 4 h) were significantly different between SCC and TB, but not easily differentiated between AC and TB. When stdSUVavg between 1–4 h was used to fit the DMCs of SCC, AC, and TB, the differences between SCC and TB were more evident, and the DMC between AC and TB were also different.

Similar studies have also been conducted on the application of curves in the differential diagnosis of diseases; for example, a study on the application of the CT spectral HU curve in the diagnosis of early cerebral ischemia showed that there was no significant difference in the CT value, when you observed the image with the naked eye, between the diseased and healthy sides during early cerebral ischemia. However, the spectral HU curve showed that the ischemic side was slightly lower than the opposite side [17]. In this study, there was no statistical difference in metabolic parameters between AC and TB, but DMC showed some differences, suggesting that DMC has good application value in the differential diagnosis of SPL.

The comprehensive analysis of the diagnostic efficacy of each metabolic parameter and DMC in this study showed that a set of stdSUVavg data had a good diagnostic efficacy, and the sensitivity and specificity of stdSUVavg at 1 h and stdSUVavg at 4 h were relatively high. ANN simulates the biological nervous system and has become increasingly important in modeling and prediction, and the prediction of complex relationships between variables is impossible for other models such as logistic regression, which is useful in clinical diagnosis, especially cancer diagnosis [18,19].

Fig. 9



SCC and TB ANN model, ROC curve is 100% (a), AC and TB ANN model-1, ROC curve is 83.5% (b), AC and TB ANN model-2, ROC curve is 87.7% (c). SCC, squamous cell carcinoma; TB, tuberculosis.

Based on the above characteristics, we selected stdSUVavg (at 1 h and 4 h), stdSUVavg slope between 1–4 h, uniformity of FDG uptake, and age to establish an ANN prediction model for SCC and TB, the positive predictive value, negative predictive value, overall accuracy, and AUC were 100.0%, suggesting that ^{18}F -FDG PET/CT MTPI has a good application value in the differential diagnosis of SCC and TB.

Although there was no statistical difference in metabolic parameters between AC and TB in this study, the curves of stdSUVavg (at 1 h, 2 h, 3 h, and 4 h) showed a certain difference; therefore, we tried to use the same indicators used in the SCC and TB models to construct a prediction model for AC and TB. The results showed a positive predictive value of 100.0%, a negative predictive value of 33.3%, an overall accuracy of 85.7%, and an AUC of 83.5%. To try to improve the diagnostic efficiency of the ANN between AC and TB, we added stdSUVavg at 2 h and stdSUVavg at 3 h to the AC and TB models, which was equivalent to the selection of all metabolic parameters related to stdSUVavg, and the AUC was increased to 87.7%.

This study also has the following shortcomings: (1) as a single-center study with a small amount of data, the results may not represent universality, and (2) the distinction between LC and inflammatory pseudotumor (IP) is also a big problem. Although we had preliminarily analyzed the DMC of IP in a previous study [3], the current collected cases of IP are too few (less than 10 cases), so no detailed analysis related to it was conducted in this study, and the identification of LC subtypes has clinical value in guiding clinical treatment [20–22]. Studies [23] have shown that the SUVmax of SCC was significantly higher than that of AC. The results suggested by the DMC in our previous study [3] and this study are consistent with the literature reports, and no comparison was made between SCC and AC. In the future, we will gradually increase the number of multicenter studies, constantly increase the sample size, and conduct more comparative studies between different pathological types of SPLs to provide more references for the accurate diagnosis of different SPLs.

In summary, for SPLs with difficult differential diagnosis, 4 h time-point scanning can be performed if time permits, and 1 h conventional scanning and 4 h delayed imaging can be selected if time does not permit. The comprehensive judgment was made by referring to the metabolic parameters at each time point, especially the threshold of stdSUVavg and the DMC, which would be of great value for the differentiation between SCC and TB, and of certain help for the differentiation between AC and TB. The establishment of ANN prediction models would significantly improve the differential diagnosis efficiency between LC and TB.

Acknowledgements

The authors thank all colleagues for their participation in this project, Xiping Shen for his guidance in statistics, and Editage for English language editing.

Table 2 Classification table of artificial neural network

Model	Sample	Observed	Predicted		Percent correct
			1/2	3	
Model-SCC vs. TB	Training	1	12	0	100.00%
		3	0	8	100.00%
	Overall percent		60.00%	40.00%	100.00%
	Testing	1	5	0	100.00%
		3	0	6	100.00%
Overall percent		45.50%	54.50%	100.00%	
Model-AC vs. TB	Training	2	21	1	95.50%
		3	3	8	72.70%
	Overall percent		72.70%	27.30%	87.90%
	Testing	2	11	0	100.00%
		3	2	1	33.30%
	Overall percent		92.90%	7.10%	85.70%

AC, adenocarcinomas; SCC, squamous cell carcinoma; TB, tuberculosis.

Table 3 Model summary

Model-SCC vs. TB	Training	Sum of squares error	0.358	
		Percent incorrect predictions	0.00%	
		Training time	00 : 00.0	
Testing	Testing	Sum of squares error	.029 ^a	
		Percent incorrect predictions	0.00%	
		Sum of squares error	4.753	
Model-AC vs. TB	Training	Percent incorrect predictions	12.10%	
		Training time	00 : 00.0	
		Sum of squares error	1.616 ^a	
	Testing	Testing	Percent incorrect predictions	14.30%

AC, adenocarcinomas; SCC, squamous cell carcinoma; TB, tuberculosis.

^aThe number of hidden units is determined by the testing data criterion: The 'best' number of hidden units is the one that yields the smallest error in the testing data.

This work was supported by the open fund project of a key laboratory of medical imaging in the Gansu province, China (Grant numbers: GSYX202008).

Conflicts of interest

There are no conflicts of interest.

References

- Cui EN, Yu T, Shang SJ, Wang XY, Jin YL, Dong Y, et al. Radiomics model for distinguishing tuberculosis and lung cancer on computed tomography scans. *World J Clin Cases* 2020; **8**:5203–5212.
- Ankrah AO, Glaudemans AWJM, Maes A, Van de Wiele C, Dierckx RAJO, Vorster M, et al. Tuberculosis. *Semin Nucl Med* 2018; **48**:108–130.
- Luo Y, Li J, Huang L, Han Y, Tian X, Ma W, et al. Value of dynamic metabolic curves and artificial neural network prediction models based on ¹⁸F-FDG PET/CT multiphase imaging in differentiating nonspecific solitary pulmonary lesions: a pilot study. *Nucl Med Commun* 2022; **43**:1204–1216.
- Boellaard R, Delgado-Bolton R, Oyen WJ, Giammarile F, Tatsch K, Eschner W, et al.; European Association of Nuclear Medicine (EANM). FDG PET/CT: EANM procedure guidelines for tumour imaging: version 2.0. *Eur J Nucl Med Mol Imaging* 2015; **42**:328–354.
- Albano D, Gatta R, Marini M, Rodella C, Camoni L, Dondi F, et al. Role of ¹⁸F-FDG PET/CT radiomics features in the differential diagnosis of solitary pulmonary nodules: diagnostic accuracy and comparison between two different PET/CT scanners. *J Clin Med* 2021; **10**:5064.
- Li Q, Li Y, Yuan H, Yang F, Huang Y, Song X, et al. PET morphology helps distinguish solitary and solid pulmonary tuberculosis from non-small cell lung cancer. *Jpn J Radiol* 2022; **41**:312–321.
- Zhou Y, Ma XL, Zhang T, Wang J, Zhang T, Tian R. Use of radiomics based on ¹⁸F-FDG PET/CT and machine learning methods to aid clinical decision-making in the classification of solitary pulmonary lesions: an innovative approach. *Eur J Nucl Med Mol Imaging* 2021; **48**:2904–2913.
- Zhao C, Deng D, Ye W, Long L, Lu Y, Wei Y. Diffusion-weighted imaging with background body signal suppression (DWIBS) distinguishes benign lesions from malignant pulmonary solitary lesions. *Am J Transl Res* 2021; **13**:88–101.
- Zhang J, Ma G, Cheng J, Song S, Zhang Y, Shi LQ. Diagnostic classification of solitary pulmonary nodules using support vector machine model based on 2-[¹⁸F]fluoro-2-deoxy-D-glucose PET/computed tomography texture features. *Nucl Med Commun* 2020; **41**:560–566.
- Cruickshank A, Stieler G, Ameer F. Evaluation of the solitary pulmonary nodule. *Intern Med J* 2019; **49**:306–315.
- Groheux D, Quere G, Blanc E, Lemaignier C, Vercellino L, de Margerie-Mellon C, et al. FDG PET-CT for solitary pulmonary nodule and lung cancer: Literature review. *Diagn Interv Imaging* 2016; **97**:1003–1017.
- Chen S, Harmon S, Perk T, Li X, Chen M, Li Y, et al. Using neighborhood gray tone difference matrix texture features on dual time point PET/CT images to differentiate malignant from benign FDG-avid solitary pulmonary nodules. *Cancer Imaging* 2019; **19**:56.
- Vorster M, Sathekge MM, Bomanji J. Advances in imaging of tuberculosis: the role of ¹⁸F-FDG PET and PET/CT. *Curr Opin Pulm Med* 2014; **20**:287–293.
- Gu J, Ren Y, Chen X, Jiang Y, Zhou W, Wang L, et al. ¹⁸F-FDG PET/CT manifestations of massive type active pulmonary tuberculosis and its differentiation from lung cancer. *Nan Fang Yi Ke Da Xue Xue Bao* 2020; **40**:49–55.
- Erdoğan M, Evrimler S, Aydın H, Karabrahimoğlu A, Şengül SS. Solitary Pulmonary Nodule: Morphological Effects on Metabolic Activity Assessment. *Mol Imaging Radionucl Ther* 2019; **28**:112–119.
- Shen CT, Qiu ZL, Sun ZK, Wei WJ, Song HJ, Zhang XY, et al. Dual time-point ¹⁸F-FDG PET/CT imaging with multiple metabolic parameters in the differential diagnosis of malignancy-suspected bone/joint lesions. *Oncotarget* 2017; **8**:71188–71196.
- Yongjun L, Hao Z, Wenjuan Z, Dan W, Qiaoying Z, Junlin Z. Plain computed tomography with spectral imaging findings of early cerebral ischemia. *J Craniofac Surg* 2020; **31**:125–129.
- Renganathan V. Overview of artificial neural network models in the biomedical domain. *Bratisl Lek Listy* 2019; **120**:536–540.
- Nair TM. Building and interpreting artificial neural network models for biological systems. *Methods Mol Biol* 2021; **2190**:185–194.
- Ma Y, Feng W, Wu Z, Liu M, Zhang F, Liang Z, et al. Intra-tumoural heterogeneity characterization through texture and colour analysis for differentiation of non-small cell lung carcinoma subtypes. *Phys Med Biol* 2018; **63**:165018.
- Zhang G, Cao Y, Zhang J, Ren J, Zhao Z, Zhang X, et al. Predicting EGFR mutation status in lung adenocarcinoma: development and validation of a computed tomography-based radiomics signature. *Am J Cancer Res* 2021; **11**:546–560.
- Huang L, Cao Y, Zhou F, Li J, Ren J, Zhang G, et al. Lung adenocarcinoma: development of nomograms based on PET/CT images for prediction of epidermal growth factor receptor mutation status and subtypes. *Nucl Med Commun* 2022; **43**:310–322.
- Tomori Y, Yamashiro T, Tomita H, Tsubakimoto M, Ishigami K, Atsumi E, et al. CT radiomics analysis of lung cancers: differentiation of squamous cell carcinoma from adenocarcinoma, a correlative study with FDG uptake. *Eur J Radiol* 2020; **128**:109032.